IUST
Iran University of Science and Technology

Iranian Journal of Electrical and Electronic Engineering

Journal Homepage: ijeee.iust.ac.ir

An Effective Hilbert–Huang Transform-Based Approach for Partial Demagnetization Fault Diagnosis in Double-Rotor Double-Sided Stator Structure Axial Flux Permanent Magnet Generator under Various Load and Speed Conditions

M. Torabi* and Y. Alinejad-Beromi*(C.A.)

Abstract: A double-sided axial flux Permanent Magnet (PM) generator which can be directly driven by small-scale low-speed turbines is highly suitable for use in renewable energy generation systems. Partial demagnetization is a failure occurring under the high thermal operation of a Permanent Magnet machine. This paper focuses on partial demagnetization fault diagnosis in a double-rotor double-sided axial flux PM generator using stator currents analysis under time-varying conditions. One of the most important problems in any fault diagnosis approach is the investigation of load and speed variation on the proposed indices. To overcome the aforementioned problems, this paper adopts a novelty detection algorithm based on the Hilbert–Huang transform for fault diagnosis. This approach relies on two steps: estimating the intrinsic mode functions (IMFs) by the empirical mode decomposition (EMD) and computing the instantaneous amplitude (IA) and Instantaneous Frequency (IF) of IMFs using the Hilbert transform. The more significant IMFs are determined using the Hilbert spectrum, which is applied for accurate fault diagnosis. The Partial demagnetization severity can be evaluated based on the IMF's energy value. The theoretical basis of the proposed method is presented. The effectiveness of the proposed method is verified by a series of simulation and experimental tests under different conditions.

Keywords: Double-Sided Axial Flux Permanent Magnet Generator, Partial Demagnetization Fault Diagnoses, Stator Currents, Hilbert–Huang Transform.

1 Introduction

PERMANENT Magnet (PM) machines have been extensively used in a variety of industrial applications and renewable energy generation due to their high power density, high efficiency, and simple controllability [1]. Among different types of PM machines, the double structural axial flux PM machine (AFPM) is applied for direct driving of small-scale low-speed turbines with wide speed variation because of its suitable performance [2, 3]. In practice, AFPMs are subjected to various mechanical faults (partial demagnetization, eccentricity and bearing fault) and electrical faults (mainly short circuit faults) occurrence. Partial demagnetization occurs due to armature reaction, temperature rise, oxidation, corrosion, structural failure, and degradation of the permanent magnet coercive force. Under partial demagnetization conditions, the stator current increases to provide the same quantity of electromagnetic torque, causing significant thermal insulation stress, which reduces their expected life [4, 5]. Moreover, partial demagnetization increases the magnitude of higher force harmonic components resulting in vibration and acoustic noise during machine operation and changing the attraction between the rotor and the

Iranian Journal of Electrical & Electronic Engineering, 2023.
Paper first received 11 Oct 2022 and accepted 13 Sep 2023.
* The authors are with the Department of Electrical Engineering, Semnan University, Semnan, Iran.
E-mails: s.makan.torabi@semnan.ac.ir, yalinejad@semnan.ac.ir.
Corresponding Author: Y. Alinejad-Beromi.

stator, causing an alteration in the machine's shaft trajectory.

Several methods have been developed for partial demagnetization fault diagnosis in AFPMs. These methods can be divided into five main categories: 1) magnetic flux analysis, 2) noise or vibration analysis, 3) torque profile analysis, 4) analytical methods based on machine modeling parameters estimation, and 5) analysis of the machine's current. The capabilities of each method for online or offline diagnosis under stationary or non-stationary conditions are different. Magnetic flux analysis is an accurate method for various fault diagnoses, including partial demagnetization fault. In [6], the electromotive force (EMF) is analyzed under partial demagnetization conditions to extract the frequency components caused by the fault, and in [7] a Back-EMF Based Method is applied for partial demagnetization fault diagnosis in permanent magnet synchronous machines. The magnetic flux signal can be driven from the induced voltage of mounted search coils [8] and the Hall Effect sensor [9-11]. The magnetic field analysis method is appropriate for online diagnosis under non-stationary conditions, but the high cost and difficulty of mounting the search coils and sensors are the main drawbacks of this method. In [12-14], the vibration signature analysis-based method is developed for machine failure monitoring, and in [15] and [16], the analysis of acoustic noise is employed to introduce an index for partial demagnetization and eccentricity fault detection. The main limitation of the vibration and acoustic analysis method is the necessity of physical access to the machine and perpetual installation of sensors, which increases the system cost and reduces system reliability. In addition, various conditions may generate similar patterns in the vibration and acoustic noise, which leads to wrong judgment. In [17], spectrum analysis of the machine current and torque is applied to online partial demagnetization fault diagnosis. Direct measurement of torque requires expensive sensors and is an invasive method. Therefore, the electromagnetic torque can be computed by considering the saturation through accurate analytical equations [18]. In [19-24], the analytical model-based method is developed for machine fault diagnosis, and in [25] the machine is modeled by using permeance network theory for demagnetization fault Identification in a permanent magnet synchronous machine. In [26], a frequency-based analytical model is proposed to investigate the demagnetization defects in AFPMSMs, and in [27], the alteration in equivalent inductance has been applied to distinguish between eccentricity and partial demagnetization. Modeling and parameter estimation methods are sensitive, reliable, and more suitable for off-line diagnosis or non-stationary machine conditions.

The Machine Current Signature Analysis (MCSA) is the most common method for fault identification. The main advantage of the MCSA method is that no expensive sensors are needed, and the applied procedures are not invasive and intricate [28-32]. In this approach, frequency analysis using the Fast Fourier Transform (FFT) is applied for fault diagnoses under stationary conditions [33]. The extended version of MCSA, Transient MCSA, is applied for fault diagnoses under non-stationary conditions. In the TMCAS procedure, time-frequency analysis methods are employed for feature extraction to fault diagnose [34, 35]. Different time-frequency analysis techniques have been recommended to apply TMCSA. Short-Time Fourier Transform (STFT) has been proposed as the developed version of Fourier transform for non-stationary signals [36, 37]. In the STFT method, the obtained signal is divided into several time periods using windows with predetermined lengths and types, and any section is analyzed by Fourier transform. The main drawback of this technique is that the type and length of the window must be selected suitably depending on the intended application and frequency components, which are not a theoretical process [38]. To analyze the signals with fast dynamics, multi-resolution signal processing methods including wavelet transform have been applied [39]. In fact, wavelet transform makes it possible to vary the time and frequency resolution on the time-frequency plane [40-42]. The main drawback of this method is that once the wavelet function is chosen, it should be applied to analyze all the sampled data. Also, in a discrete wavelet with permanent sampling, frequency bands of scales are dependent on sampling frequency.

Recently, the Hilbert-Huang transform (HHT) as a novel approach has been investigated for machine fault diagnoses under non-stationary conditions. In [43] and [44], the HHT has been applied for broken

rotor bars and bearing fault detection in an induction machine. The use of HHT for stator fault identification in PM synchronous machines with radial flux structure has been provided in [45] and [46].

Load and speed variation, along with partial demagnetization fault, directly affects the behaviors of partial demagnetization signatures that appear in the current spectrum of the generator. Such a problem is one of the most important problems in any fault diagnosis approach.

In this paper, a novelty detection algorithm based on the Hilbert–Huang transform is provided to overcome the aforementioned problems for accurate partial demagnetization diagnosis in a double-structural AFPM generator. To evaluate the validity of the proposed method, simulation, and experiments for unsteady speed in the presence of linear and non-linear load under healthy and different demagnetization severity conditions of the generator have been performed.

The contributions of this paper can be expressed as follows:

1) Compared with the existing demagnetization diagnosis method, the proposed method provides a more reliable and accurate evaluation of demagnetization fault occurrence when the stator currents are not sinusoidal due to the harmonics caused by non-linear loads, in such a way that the applied technique makes it easier the extraction of demagnetization signatures by rejecting the load related components and other undesired frequencies.

2) As the fault-related signatures at the initial stages of the fault occurrence are very weak and also are chaotic due to load and speed variations, the proposed approach in comparison to other MCSA methods, provides a more robust diagnosis by tracking the faulty frequencies using an effective HHT-based technique.

Moreover, the energy of the introduced fault index increases with respect to fault severity and the demagnetization degree can be evaluated based on the fault components' energy value.

This paper is organized as follows. Section 2 presents the theoretical analysis of partial demagnetization in a double structural axial flux PM generator. In section 3, the HHT and its application for partial demagnetization diagnosis under non-stationary conditions are introduced. The simulation and experimental validation results that prove the effectiveness of the proposed method are elaborated in section 4. Finally, section 5 concludes the paper.

2 Theoretical Analysis of Partial Demagnetization Fault in the AFPM Generator

The double-sided topology of the AFPM generator in the 3D plane is shown in Fig. 1a, which is simulated in MAXWELL FEM software. The test generator used in this research consists of two rotor discs with surface-mounted permanent magnets and a double-side stator with series-connected four coils per phase. The back EMF is generated in the coils due to the rotation of the rotor magnets. The coils have been located in the stator slots in such a way that the direction of air gap flux density is mainly axial, as shown in Fig. 1b [47].

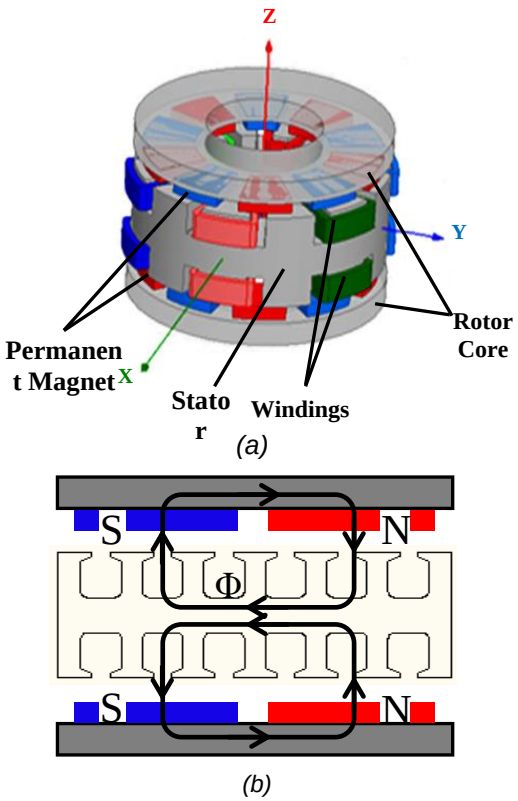

Fig. 1 AFPM generator: a) Double-sided topology in 3D plane, and b) Flux directions.

Partial demagnetization usually originates from defective manufacturing of the PMs or high loading and thermal stress. Under demagnetization conditions, the rotor magnetic field symmetry is lost and extra harmonics in stator current appear. To realize the signatures induced to the stator coil caused

by the demagnetization fault, the air-gap magnetic flux density needs to be extracted, and it is given by equation (1):

$$B_{AG(dmg)} = \Lambda_{dmg}.F_m \tag{1}$$

The magneto-motive force F_m developed from the PMs can be presented using Fourier series composition as follows [48]:

$$F_m(\theta,t) = \sum_{n=2m+1}^{\infty} F_{PM}\cos(np\theta - n\omega_s t - \varphi_n) \tag{2}$$

where m=0,1, 2, …, F_{PM}, φ_n, p, θ, ω_s, and t are the magnitude, phase angle of the MMF for the n^{th} contextually harmonic component, the number of pole pairs, an angle from a reference axis, angular electrical speed and the time variable.

The permeance due to one partial demagnetized magnet is described by [48]:

$$\Lambda_{dmg}(\theta,t) = \alpha + \beta(D) + \gamma(D)\sum_{k=1}^{\infty}\cos(k\theta - k\omega_r t) \tag{3}$$

where $\omega_r = \frac{\omega_s}{p}$ is the mechanical speed and:

$$\alpha = \frac{\mu_0}{2h_{PM}}\left(1 - \frac{g}{h_{PM}} - \frac{t_w}{2h_{PM}} + \frac{g^2}{h_{PM}^2} + \frac{gt_w}{h_{PM}^2} + \frac{t_w^2}{4h_{PM}^2}\right) \tag{4}$$

$$\beta(D) = \frac{\mu_0 D}{2h_{PM}}\left(\frac{g}{2h_{PM}^2 p} + \frac{t_w}{4h_{PM}p} - \frac{1}{2h_{PM}p}\right) \tag{5}$$

$$\gamma(D) = \frac{\mu_0}{2h_{PM}}\left\{\left(\frac{D}{2h_{PM}p} + \frac{2g}{h_{PM}} + \frac{t_w}{h_{PM}} - 1\right)\sum_{k=1}^{\infty}\frac{D}{k\pi h_{PM}}\sin\left(\frac{k\pi}{2p}\right)\right\} \tag{6}$$

where h_{PM}, g, and t_w are the magnet height, air-gap length, and the stator winding thickness. $D = \varepsilon g$ where $\varepsilon > 1$, is considered a factor that related directly to the fault severity.

Considering (1), (2) and (3), the air-gap magnetic flux density is given by:

$$B_{AG(dmg)}(\theta,t) = \sum_{n=2m+1}^{\infty} F_{PM}\cos\left(np\theta - n\omega_s t - \varphi_n\right) + \beta_k\sum_{n=2m+1}^{\infty}\sum_{k=1}^{\infty}\left\{F_{PM}\alpha_k\left[\begin{array}{l}\cos\left((np-k)\theta - \left(n-\frac{k}{p}\right)\omega_s t - \varphi_n\right) + \\ \cos\left((np+k)\theta - \left(n+\frac{k}{p}\right)\omega_s t - \varphi_n\right)\end{array}\right]\right\} \tag{7}$$

where

$$\alpha_k = \alpha + \beta(D) \tag{8}$$

$$\beta_k = \frac{\gamma(D)}{2} \tag{9}$$

The magnetic flux can be calculated by:

$$\varphi = \int\int Bds \tag{10}$$

Due to Faraday's Law, the voltage will be induced in the stator coils caused by the change in the magnetic flux:

$$e_{ind} = -N\frac{d\varphi}{dt} \tag{11}$$

Considering (7), (10), and (11) together, the induced voltage in the stator coils due to the demagnetization is described by:

$$V_{dmg} = \sum_{n=2m+1}^{\infty} V_n\cos(np\theta - n\omega_s t - \varphi_n) + \sum_{n=2m+1}^{\infty}\sum_{k=1}^{\infty} V_{nk}\left\{\left[\begin{array}{l}\cos\left((np-k)\theta - \left(n-\frac{k}{p}\right)\omega_s t - \varphi_n\right) + \\ \cos\left((np+k)\theta - \left(n+\frac{k}{p}\right)\omega_s t - \varphi_n\right)\end{array}\right]\right\} \tag{12}$$

According to [48] harmonic components that are triple multiples of the mechanical frequency cancel out in the stator current when all three phases are considered in a PM machine, where each phase consists of a single coil. If each phase consists of more coils in the three-phase system, then the demagnetization impact on each phase is [48]:

$f_{dmg1} = \left(n \pm \frac{2^{\delta}\varepsilon}{p}\right) f_s$, if the phase coils are a power of 2 (defined by δ) and n is an integer odd number.

$f_{dmg2} = \left(n \pm \frac{3k}{p}\right) f_s$, if the phase coils number is a multiple of 3 and n is an integer odd number.

Moreover, the harmonics obeying $f_{3ph\_null} = \frac{3\gamma\lambda'}{p} f_s$ (γ is the number of phase coils and $\lambda' \in Z$) are canceled out due to the spatial phase difference between coils of three-phase winding [48]. It means that, for a machine with 2 coils per phase, the sixth multiples of the mechanical frequency will not exist in a 3-phase PM generator due to the demagnetization. If phase winding consists of 4 coils the twelfth multiples of the mechanical frequency cancel out etc.

3 Partial Demagnetization Diagnoses Based on Hilbert-Huang Transform

The Hilbert-Huang Transform (HHT) is the expansion of the Hilbert transform for non-linear and non-stationary signal analysis. The HHT consists of two parts: empirical mode decomposition (EMD) and Hilbert spectral analysis (HSA). The EMD is applied to decompose the main signal into monotonic frequency components, known as intrinsic mode function (IMF). The obtained signatures of the Hilbert transform of the IMFs are used as features for fault diagnosis.

This section presents the use of HHT for axial flux generator stator currents analysis in non-stationary conditions.

3.1 Empirical Mode Decomposition

The applications of the Hilbert transform are all limited to mono-component functions with only one frequency value at any given time; hence, the EMD method is necessary to deal with multi-component signals from non-stationary and nonlinear processes. The EMD is defined by an algorithm, as in the following steps [49]:

1) Identification of all extrema (local minima and local maxima points) of actual signal x[n].

2) Connecting all local minima (resp. all local maxima) to produce the lower and upper envelope ($e_{min}[n]$ and resp.$e_{max}[n]$).

3) Extraction of the mean as:

$$m[n] = \frac{e_{min}[n] + e_{max}[n]}{2} \quad (13)$$

4) Computation of the detail as:

$$d[n] = x[n] - m[n] \quad (14)$$

5) Algorithm iteration by considering d[n] instead of x[n] (sifting process).

The algorithm has to be refined by repeating the sifting process until two conditions are fulfilled [49]:

1) The number of extrema and the quantity of zero-crossings should either equal or differ at most by one.

2) The mean value of the lower and upper envelopes should be close to zero.

After this procedure, the detail d[n] corresponds to the first Intrinsic Mode Function (IMF1) which is named c_1, and the residue r_1 is defined as:

$$r_1[n] = x[n] - c_1[n] \quad (15)$$

r_1 is treated as the new actual data (instead of x[n]) and subjected to the same sifting process as described above. This procedure is repeated to extract more IMFs. The sifting process can be stopped finally by any of the following predetermined criteria: 1. when the component $C_i[n]$ or the residue $r_i[n]$ becomes so small that it is less than the predetermined value of substantial consequence; or 2. when the residue $r_i[n]$ becomes a monotonic function from which no more IMFs can be extracted.

3.2 Instantaneous Amplitude (IA) and Frequency (IF) Extraction by The Hilbert Transform (HT)

The IA and IF of each IMF are computed using the Hilbert transform. When the EMD is jointly applied with the Hilbert transform, the transformation is named the HHT. The discrete definition of the Hilbert transform is formulated as:

$$x^h[n] = x[n] * h[n] \quad (16)$$

where $*$ points to the convolution product. The superscript in $X^h[n]$ denotes the Hilbert transform of the sampled stator current x[n], and:

$$h[n] = \begin{cases} 0 & for\ even\ n \\ \frac{2}{n\,\pi} & for\ odd\ n \end{cases} \quad (17)$$

The analytic signal is defined as:

$$z^h[n] = x[n] + jx^h[n] = a[n]e^{j\theta[n]} \quad (18)$$

The instantaneous amplitude (IA) and the instantaneous frequency (IF) are given by:

$$\hat{a}[n] = |z^h[n]| \quad (19)$$

$$\hat{f}[n] = \frac{1}{2\pi}\left(\angle(z^h[n+1]) - \angle(z^h[n])\right) \times F_s \quad (20)$$

where $|z^h[n]|$ and $\angle(z^h[n])$ are the moduli and the argument of complex-valued signal $z^h[n]$ respectively and F_s is the data sampling rate. Finally, the time-frequency distribution is obtained by displaying the time evolution of the instantaneous amplitude and frequency for each IMF in the time-frequency plane.

3.3 HHT-Based Algorithm for Partial Demagnetization Diagnoses in AFPMs

The proposed procedure for partial demagnetization diagnoses in AFPMs is represented in Fig. 2. The fault components will be derived using EMD in the presence of a partial demagnetization fault. After signal decomposition to its components, the Hilbert transform is used to compute the instantaneous amplitude (IA) and the Instantaneous Frequency (IF) of each IMF. In fact, the Hilbert transform converts the local energy and IF extracted from the IMFs to a full-energy-frequency-time distribution of the signal, with energy defined as the amplitude squared [50]. The signal energy is represented by the joint function of time and the IF. Such a representation is named Hilbert spectrum. The more significant IMFs caused by faulty conditions are determined using the Hilbert spectrum, which are considered partial demagnetization indicators.

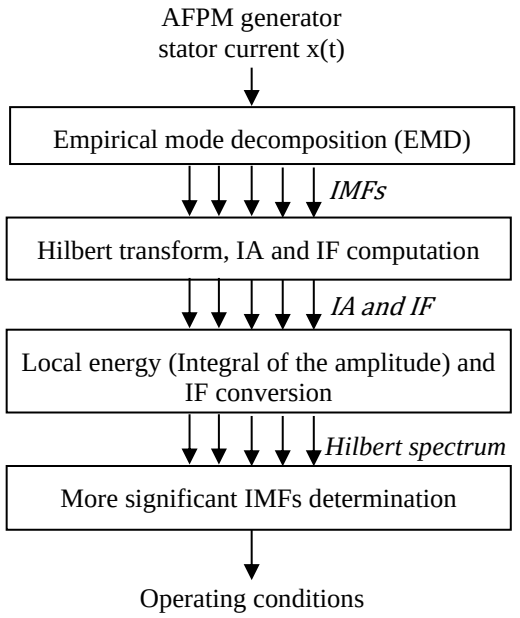

Fig. 2 The proposed algorithm for partial demagnetization diagnoses in AFPMs.

4 Simulation and Experimental Results

To validate the usefulness of the proposed method, a series of simulations and experiments have been carried out on a double-sided AFPM generator (Fig. 3a and Fig. 3b) in healthy and faulty states under various conditions. The experimental setup for data sampling, including AC motor (with speed control drive), AFPM generator, oscilloscope, and variable load is shown in Fig. 3c. The constructed generator characteristics are listed in Table 1.

In the experimental setup, partial demagnetization is caused by the single defective permanent magnet on both sides of the rotor, which can be implemented by heating the PM pieces. This is done via hot oil as shown in Fig. 3. The magneto motive Force of defected PM pieces is evaluated by a Hall-Effect sensor with analogue output.

For a comprehensive method survey, the simulations and experiments have been done on the investigated AFPM at unsteady speed with linear and non-linear load under healthy and faulty conditions of the generator with different demagnetization severities.

AFPM at unsteady speed with linear and non-linear load under healthy and faulty conditions of generator with different demagnetization severities.

Table 1 AFPM Generator characteristics table.

Phase EMF (RMS) @ 600rpm	81.42	v
Outer diameter of stator	132`	mm
Inner diameter of stator	25	mm
Air gap length	1.2	mm
Machine mechanical rated speed	500	rpm
Number of coils per each side of stator	6	
Number of coils on double sided stator	12	
Number of PM pieces on a rotor disk	10	
Number of PM pieces in generator	20	
Electrical frequency	50	Hz
Rated phase current (RMS)	1.2	A
Rated output power	100	w
Number of conductors turns per coil	180	
Conductor diameter	0.55	mm
PM pieces class	N52 MGOe	
Magneto motive Force of PM pieces	923000	At

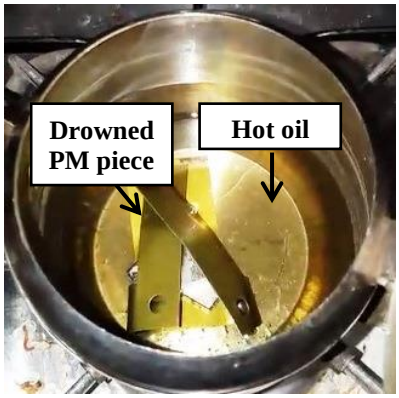

Fig. 3 PM pieces demagnetizing using the hot oil.

For a comprehensive method survey, the simulations and experiments have been done on the investigated AFPM at unsteady speed with linear and non-linear load under healthy and faulty conditions of the generator with different demagnetization severities.

Considering the generator structure there are 2 phase coils at 180 degrees apart (2 coils per phase on each side of the stator). Therefore, as described earlier the demagnetization will produce current harmonics around the fundamental at frequencies $\left(n \pm \frac{2\varepsilon}{5}\right) f_s$ ($\left(n \pm \frac{2^\delta \varepsilon}{p}\right) f_s$, $2^\delta = 2$, $p = 5$ and n is an integer odd number:

$$\left(3-\frac{2}{5}\right)f_s,\quad \left(3-\frac{4}{5}\right)f_s,\quad \left(3-\frac{6}{5}\right)f_s,\quad \left(3-\frac{8}{5}\right)f_s,$$
$$\left(3-\frac{10}{5}\right)f_s,\quad \left(3-\frac{12}{5}\right)f_s,\quad \left(3-\frac{14}{5}\right)f_s,\quad \left(1-\frac{2}{5}\right)f_s,$$
$$\left(1-\frac{4}{5}\right)f_s,\quad \left(1+\frac{2}{5}\right)f_s,\quad \left(1+\frac{4}{5}\right)f_s,\quad \left(1+\frac{6}{5}\right)f_s,$$
$$\left(1+\frac{8}{5}\right)f_s,\quad \left(1+\frac{10}{5}\right)f_s,\quad \left(1+\frac{12}{5}\right)f_s,\quad \left(1+\frac{14}{5}\right)f_s,$$
$$\left(1+\frac{16}{5}\right)f_s,\quad \left(1+\frac{18}{5}\right)f_s,\quad \left(1+\frac{20}{5}\right)f_s,\quad \left(3+\frac{2}{5}\right)f_s,$$
$$\left(3+\frac{4}{5}\right)f_s,\quad \left(3+\frac{6}{5}\right)f_s,\quad \left(3+\frac{8}{5}\right)f_s,\quad \left(3+\frac{10}{5}\right)f_s,$$
$$\left(3+\frac{12}{5}\right)f_s.$$

Moreover, the signatures at frequencies $\frac{6\lambda'}{5}f_s$ ($\frac{3\gamma\lambda'}{p}f_s$, $\gamma = 2$ and $p = 5$) are canceled out in the stator current. So, under partial demagnetization conditions, the signatures that the test generator is expected to have around the fundamental frequency of the stator current (50Hz) appear as:

$$\left(\frac{1}{5}\right)f_s,\ \left(\frac{3}{5}\right)f_s,\ \left(\frac{7}{5}\right)f_s,\left(\frac{9}{5}\right)f_s,\ \left(\frac{11}{5}\right)f_s,\ \left(\frac{13}{5}\right)f_s,\ \left(\frac{17}{5}\right)f_s,$$
$$\left(\frac{19}{5}\right)f_s,\left(\frac{21}{5}\right)f_s,\left(\frac{23}{5}\right)f_s,\left(\frac{27}{5}\right)f_s$$

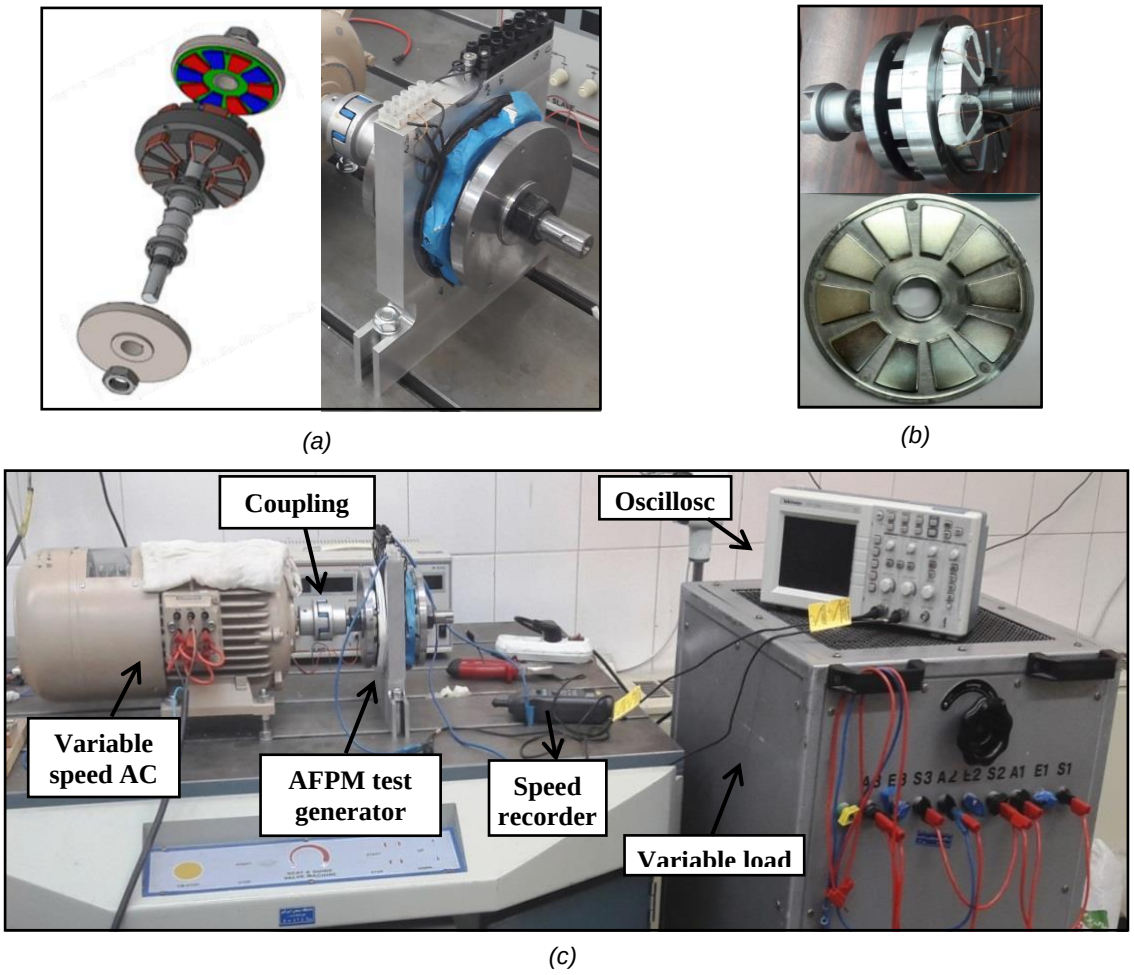

Fig. 4 a) Exploded view drawing of the generator and assembled AFPM, b) Stator core with two installed coil and Rotor disk with PM pieces, and c) Practical setup for experimental data sampling.

Although partial demagnetization usually occurs non-uniformly, a local defect on a single permanent magnet with 36% and 60% demagnetization on both sides of the rotor is considered. The stator currents have been recorded during 3.5 seconds with a 1 kHz sampling rate (Fig. 5a and Fig. b). The experimental results are compared to those of the simulation tests and the expectations of theoretical analysis. Fig. 5c gives a series of computed IMFs extracted from the original signal of the actual generator under faulty conditions with demagnetization severity of 60% at speed variations of 0% to nominal speed in the presence of a linear load. These IMFs have been generated at frequencies $\left(n \pm \frac{2\varepsilon}{5}\right) f_s$ (10Hz, 30Hz, 70Hz, 90Hz, 110Hz, 130Hz, 170Hz, 190Hz, 210Hz, 230Hz and 270Hz at nominal speed) due to partial demagnetization faults. The more significant IMFs caused by the faulty conditions are determined by means of the Hilbert spectrum, which are applied for partial demagnetization identification.

For instance, Fig. 6 gives the Hilbert spectrum of stator current under healthy and partial demagnetization conditions at speed variations of 0% to nominal speed in the presence of a linear load. The color bar in the Hilbert spectrum presents the energy levels in A^2 (amplitude squared). The amplitude of fault components is small in comparison to the amplitude of the fundamental harmonics, thus to increase the resolution of T-F (time-frequency) distributions, the fundamental, 3rd, 5th, and 7th harmonics have been removed by EMD and cannot be seen on IMF1 to IMF11. It makes the appearance of fault components in the Hilbert spectrum easier. As shown in Fig. 6a and Fig. 6b, only the fundamental and sub-harmonics (3rd, 5th, and 7th) can be seen in the Hilbert spectrum under healthy conditions and no-fault components have appeared. Fig. 6c and Fig. 6d show the energy of IMFs affected by partial demagnetization.

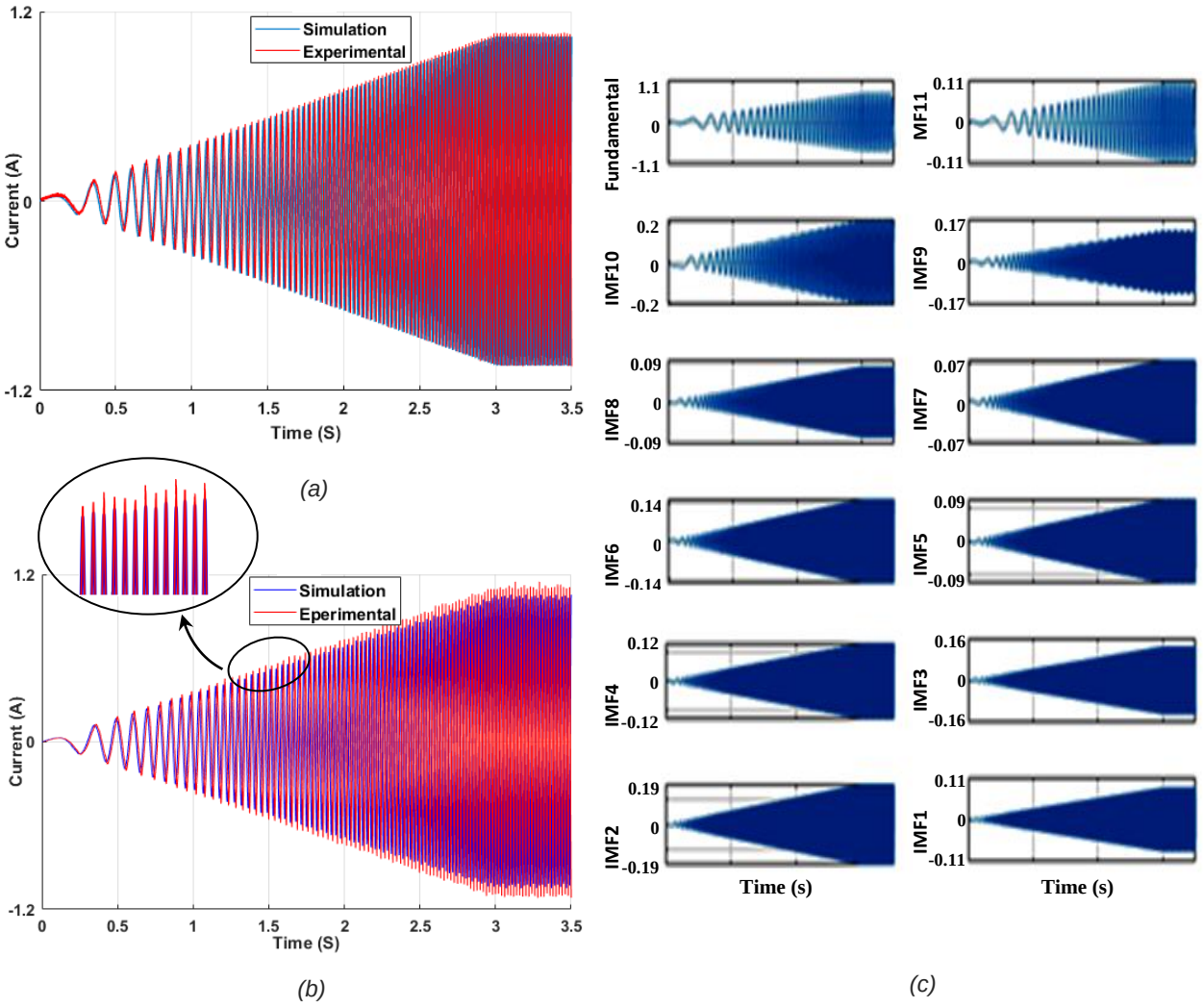

Fig. 5 Simulated and experimental stator current (with a linear load) a) Healthy condition, b) Faulty condition with demagnetization severity of 60%, and c) A series of computed IMFs under faulty condition with demagnetization severity of 60%.

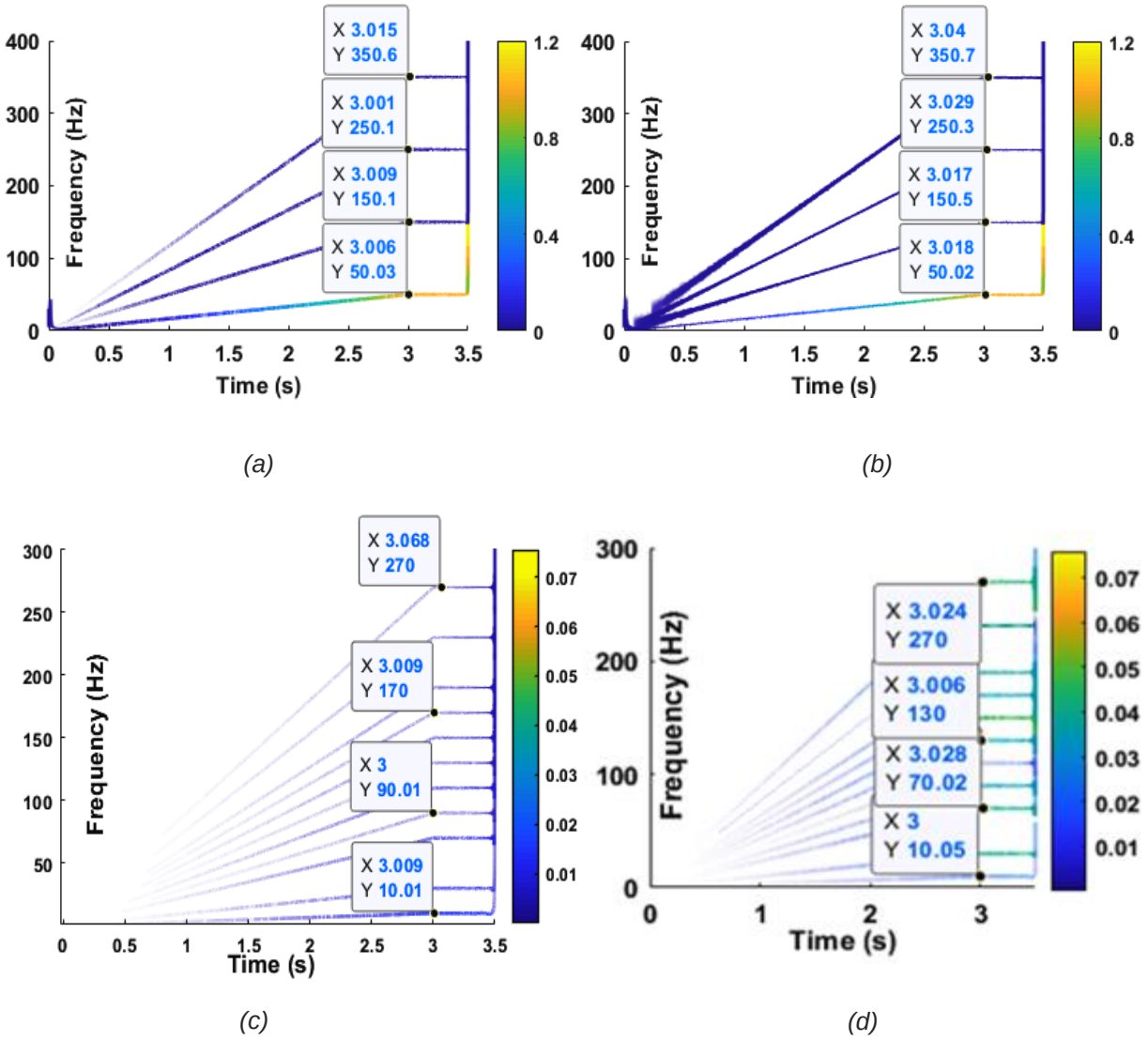

Fig. 6 Hilbert spectrum of stator current (with a linear load) a) Simulated healthy condition, b) Actual healthy condition, c) Simulated faulty condition with demagnetization severity of 60%, and d) Actual faulty condition with demagnetization severity of 60%.

Table 2 gives the Instantaneous Frequency (IF) of simulated and experimental stator current components under partial demagnetization conditions in the presence of a linear load with fault severities of 36% and 60%. The table is divided into four subsets based on the various generator speeds at 50, 150, 300, and 500 RPM. The phase currents are sampled at different speeds and fault severity to obtain the frequency spectrum of phase currents using the Hilbert-Huang Transform.

As it can be seen in Table 2, in addition to the fundamental component and its harmonics, the current components (affected by partial demagnetization) at frequencies $\left(n \pm \frac{2^{\delta}\varepsilon}{p}\right) f_s$ (The instantaneous fundamental frequency depends on instantaneous rotor speed) will appear together in the presence of partial demagnetization fault.

Table 2 The Instantaneous Frequency of the simulated and experimental stator current components under partial demagnetization conditions in the presence of a linear load.

Fault severity			demagnetization severity of 36%								demagnetization severity of 60%							
Test condition			Simulation				Experimental				Simulation				Experimental			
operating speed / nominal speed			**10 %**	**30 %**	**60 %**	**100 %**	**10 %**	**30 %**	**60 %**	**100 %**	**10 %**	**30 %**	**60 %**	**100 %**	**10 %**	**30 %**	**60 %**	**100 %**
Stator current components	**harmonics**	Fund	4.82	15.08	30.53	50.23	5.12	14.88	30.24	50.13	4.93	15.17	30.31	50.12	5.14	14.97	30.13	50.21
		3rd	15.01	44.83	90.21	150.2	15.21	44.91	90.11	149.2	15.13	44.74	90.13	150.2	14.84	44.82	90.24	149.8
		5th	25.04	75.46	149.8	250.3	24.73	74.86	150.1	250.2	25.14	75.37	150.1	250.1	24.85	74.91	150.2	250.3
		7th	34.83	104.7	210.4	350.1	35.13	105.2	210.1	349.9	34.91	104.8	210.3	350.3	35.22	105.1	210.2	349.9
	IMFs	IMF 1	0.99	3.37	6.05	10.12	1.09	3.15	5.93	9.82	1.09	3.28	6.16	10.17	1.18	3.17	5.86	9.93
		IMF 2	3.32	9.16	18.02	30.27	3.12	8.96	17.93	30.14	3.22	9.25	18.13	30.16	3.21	9.06	18.24	30.11
		IMF 3	7.4	21.21	42.12	70.54	7.13	21.32	41.92	69.93	7.14	21.34	42.23	70.13	7.24	21.24	41.81	69.89
		IMF 4	9.13	27.34	54.46	90. 18	8.83	26.79	53.81	90.21	9.23	27.32	54.35	90. 27	8.92	26.83	53.92	90.12
		IMF 5	11.23	33.16	66.59	110.4	11.14	32.93	66.18	110.4	11.16	33.28	66.23	110.1	11.13	32.72	66.21	110.2
		IMF 6	13.31	39.32	78.28	130.2	13.12	39.14	78.13	130.2	12.89	39.24	78.17	130.1	13.09	39.21	78.21	130.1
		IMF 7	17.21	51.17	102.3	170.3	17.09	51.08	102.1	169.3	17.12	51.26	102.21	170.2	17.18	51.23	102.3	169.2
		IMF 8	19.23	57.12	114.2	190.5	19.16	56.82	114.4	190.6	19.14	57.23	114.2	190.3	19.21	56.91	114.2	190.1
		IMF 9	20.95	63.19	126.1	210.3	21.15	62.87	126.18	210.2	20.83	63.28	126.2	210.1	21.23	62.76	126.3	210.3
		IMF 10	23.13	69.17	138.1	230.1	23.24	69.23	138.1	229.9	23.04	69.26	138.1	230.2	23.12	69.32	138.4	230.1
		IMF 11	26.8	81.18	162.3	270.2	27.16	81.31	162.1	270.1	27.05	81.23	162.2	270.3	27.14	81.21	162.2	270.1
			Instantaneous Frequency (IF) (Hz)															

Fig. 7a to Fig. 7 gives the energy values of the simulated and experimental stator current components under partial demagnetization conditions in the presence of a linear load with fault severities of 36% and 60%. The faulty condition is decomposed into four parts at 10%, 30%, 60%, and 100% of nominal speed. The energy value is defined as the amplitude squared multiplied by 10^{+6}.

As can be seen in Fig. 7a to Fig. 7d, the HHT allows removing the undesired frequencies in both an easy and fast way. It makes it possible to observe the

more important IMFs individually to increase the precision in the fault diagnosis. As shown, the energy of fault components increases with respect to fault severity. Moreover, it seems that the 2nd and 10th IMFs are the most affected IMFs and the energy of these IMFs is more reliable as a fault indicator and its severity at different rotor speeds.

Accurate fault diagnosis is questionable without investigating the relationship between the load condition and the current frequency pattern. Therefore, further results are presented here to validate the proposed technique in the presence of a non-linear load. Based on the aforementioned proved formula, the number of poles and supply frequency (depending on rotor speed) change the fault components. The same frequency components that are affected by partial demagnetization may be introduced by non-linear loads, so some harmonics can be observed in both healthy and partial demagnetization conditions. Fig. 8a and Fig. 8b give the simulated and experimental stator current at unsteady speed with a non-linear load under healthy and partial demagnetization conditions of the generator in the presence of a non-linear load with fault severity of 60%. The Hilbert spectrum of experimental stator current under healthy conditions is shown in Fig. 8c.

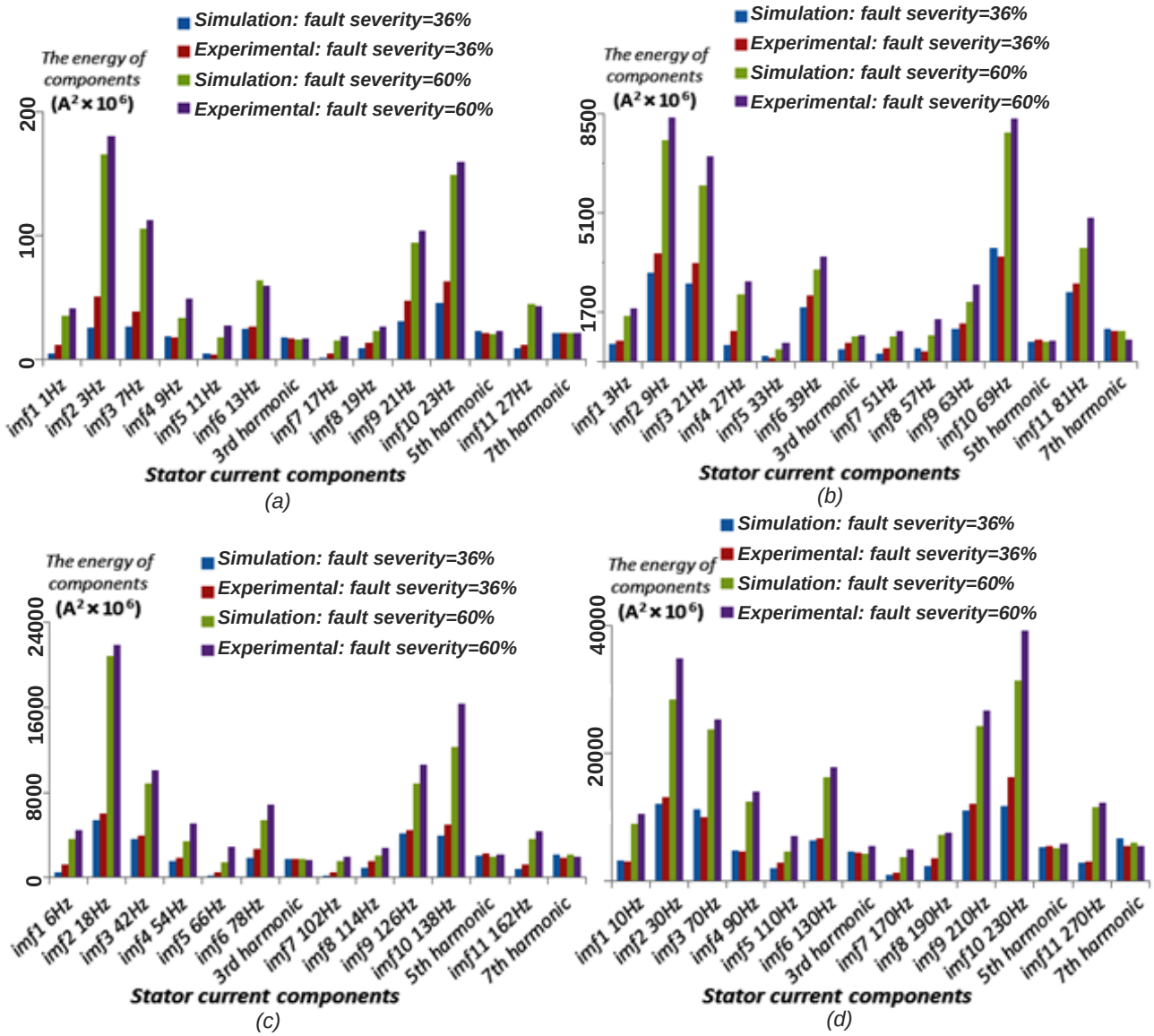

Fig. 7 Current components under partial demagnetization condition with a linear load a) at 10% of the nominal speed, b) at 30% of the nominal speed, c) at 60% of the nominal speed and d) at the nominal speed.

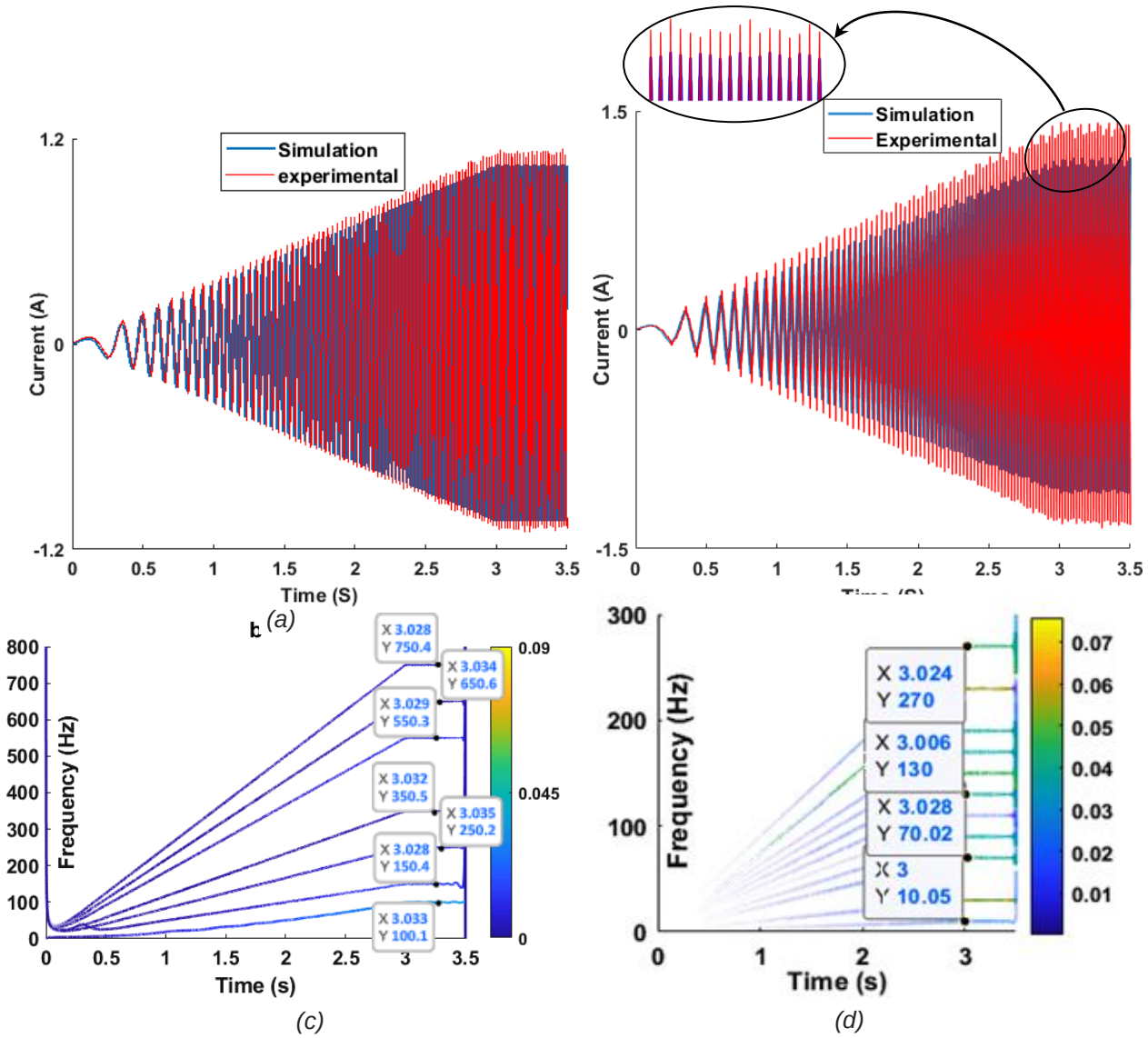

Fig. 8 Simulated and experimental stator current (with a non-linear load): a) Healthy condition, b) faulty condition with demagnetization severity of 60% Hilbert spectrum of stator current (with a non-linear load), c) Actual healthy condition, and d) Actual partial demagnetization condition**.**

As seen, the presence of non-linear load leads to harmonics (2nd, 11th, 13th, and 15th) associated with the switching operation of the converters. The amplitude of switching harmonics is small in comparison to the amplitude of the fundamental component; thus, to increase the resolution of T-F distributions, the fundamental harmonic has been removed by EMD and cannot be seen in the Hilbert spectrum. Fig. 8d shows the fault components of the experimental stator current in the Hilbert spectrum under partial demagnetization condition with fault severity of 60%. As shown, the EMD process does clear the signal from the effects of switching operation in non-linear loads for reliable and accurate fault identification. Table 3 gives the Instantaneous Frequency (IF) of the simulated and experimental stator current components under partial demagnetization conditions in the presence of a non-linear load with fault severities of 36% and 60%. As it can be seen, in addition to the fundamental component and switching harmonics, the current components (affected by partial demagnetization) at frequencies $\left(n \pm \frac{2^{\delta}\varepsilon}{p}\right) f_s$ (The instantaneous fundamental frequency depends on instantaneous rotor speed) will appear together in the presence of partial demagnetization fault.

Table 3 The Instantaneous Frequency of the simulated and experimental stator current components under partial demagnetization conditions in the presence of a non-linear load

Fault severity			demagnetization severity of 36%								demagnetization severity of 60%							
Test condition			Simulation				Experimental				Simulation				Experimental			
operating speed / nominal speed			**10 %**	**30 %**	**60 %**	**100 %**	**10 %**	**30 %**	**60 %**	**100 %**	**10 %**	**30 %**	**60 %**	**100 %**	**10 %**	**30 %**	**60 %**	**100 %**
Stator current components	**harmonics**	Fund	5.17	15.24	30.43	50.23	5.12	14.88	30.24	50.13	4.93	15.17	30.31	50.12	5.14	14.97	30.13	50.21
		3rd	55.12	165.3	330.2	550.2	15.21	44.91	90.11	149.7	15.13	44.74	90.13	150.2	14.84	44.82	90.24	149.8
		5th	65.04	195.4	389.8	650.3	24.73	74.86	150.1	250.2	25.14	75.37	150.1	250.1	24.85	74.91	150.2	250.3
		7th	74.89	224.7	450.3	750.2	35.13	105.1	210.2	349.8	34.91	104.8	210.3	350.2	35.22	105.1	210.3	349.9
	IMFs	IMF 1	1.03	3.17	6.27	10.16	1.21	3.26	5.92	9.93	1.07	3.26	6.16	10.23	1.05	3.26	5.83	9.78
		IMF 2	3.13	9.14	18.24	30.25	3.12	9.17	18.33	30.11	3.21	9.25	18.13	30.16	3.21	8.82	17.82	30.23
		IMF 3	7.23	21.23	42.32	70.24	7.15	21.13	41.78	69.89	7.27	21.32	42.23	70.43	7.24	21.41	41.78	69.82
		IMF 4	9.31	27.21	54.24	90.16	8.89	26.92	53.89	90.12	9.24	27.16	54.34	90.27	8.92	26.86	53.72	90.31
		IMF 5	11.21	33.16	66.14	110.2	11.24	32.84	66.14	110.2	11.32	33.25	66.43	110.3	11.23	32.82	66.21	110.2
		IMF 6	12.91	39.15	78.28	130.2	13.17	39.32	78.32	130.1	13.22	39.24	78.17	130.1	13.27	39.23	78.25	130.3
		IMF 7	17.21	51.15	102.32	170.1	17.27	51.32	102.2	169.2	17.33	51.26	102.21	170.2	17.34	51.19	102.3	169.2
		IMF 8	19.22	57.32	114.3	190.2	19.13	56.84	114.1	190.1	19.34	57.23	114.3	190.3	19.28	56.91	114.1	190.3
		IMF 9	20.92	63.37	126.1	210.3	21.32	62.87	126.4	210.2	20.85	63.28	126.2	210.2	21.37	62.78	126.3	210.2
		IMF 10	23.13	69.15	138.2	230.2	23.23	69.41	138.3	230.1	23.41	69.24	138.4	230.2	23.13	69.31	138.2	229.8
		IMF 11	27.15	81.34	162.3	270.1	27.25	81.12	162.2	270.1	26.79	81.27	162.1	270.3	27.29	81.27	162.4	269.9
			Instantaneous Frequency (IF) (Hz)															

Fig. 9a to Fig. 9d give the energy values of the simulated and experimental stator current components under partial demagnetization in the presence of a non-linear load with fault severities of 36% and 60%. The faulty condition is decomposed into four parts at 10%, 30%, 60%, and 100% of nominal speed. Similar to the linear load condition, the current frequency pattern is speed-dependent and the components' energy values increase almost linearly with respect to the speed and fault severity. As it has been demonstrated in this section, under non-stationary conditions with linear or non-linear load the stator current would have to be filtered by means of the EMD to remove the fundamental and other sub-harmonics prior to the applications of the fault diagnosis algorithm. This filtering increases the resolution of TF distributions and makes easier the identification of fault metrics.

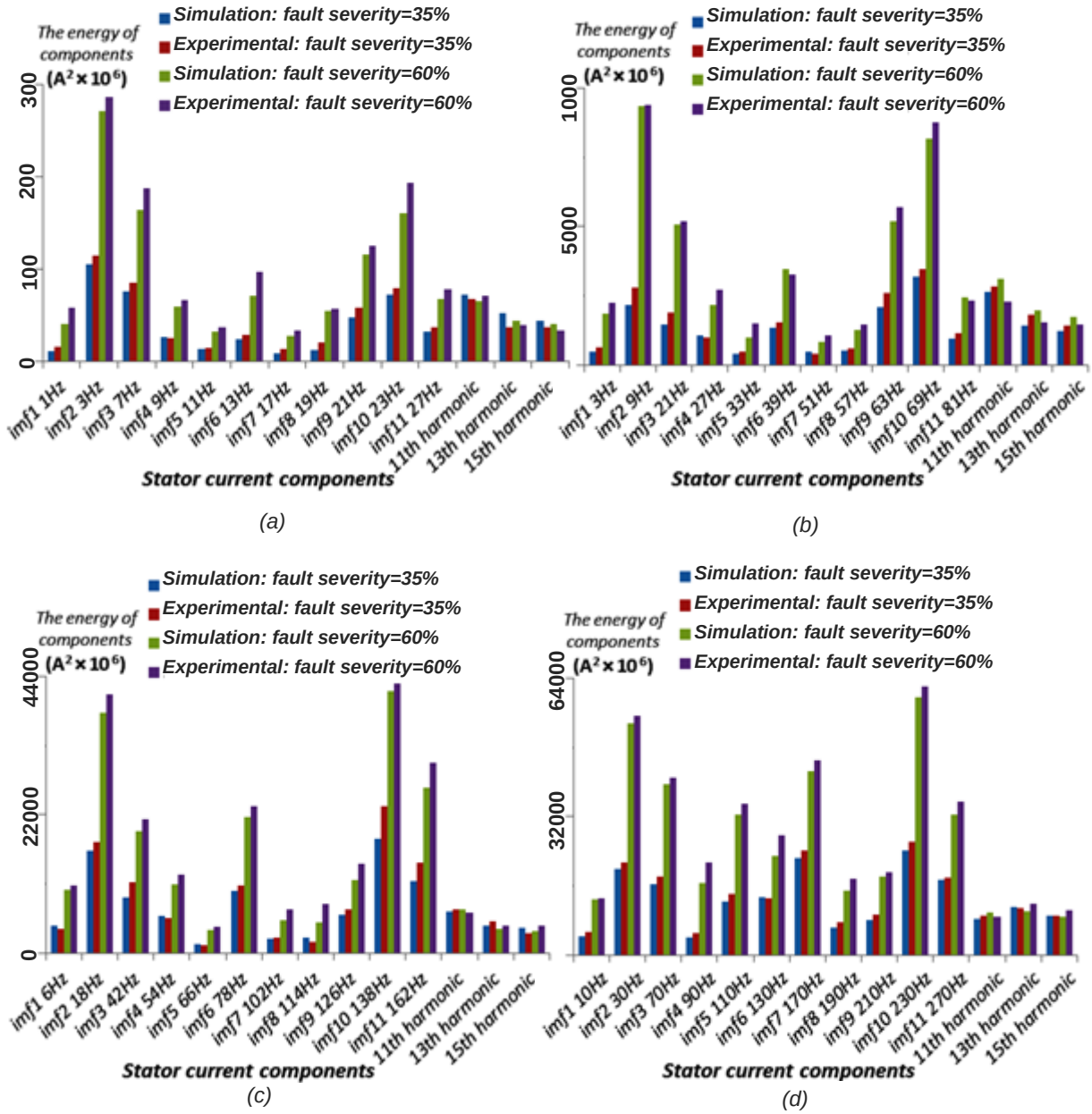

Fig. 9 Current components under partial demagnetization condition with a non-linear load a) at 10% of the nominal speed, b) at 30% of the nominal speed, c) at 60% of the nominal speed and d) at the nominal speed.

5 Conclusion

In this paper, the mathematical foundations of partial demagnetization and Hilbert–Huang transform have been settled and the use of HHT for partial demagnetization diagnosis in double-rotor double-sided stator structure AFPM generator has been investigated. As it was explained, one of the most considerable problems in any fault detection approach is the investigation of load and speed variation on the proposed indices. The usefulness of the novelty fault diagnosis algorithm based on the Hilbert–Huang transform for solving the aforementioned problems has been demonstrated on simulated and actual axial flux generators under non-stationary conditions. The results show that the HHT provides an evaluation of partial demagnetization fault occurrence when the stator currents are not absolutely sinusoidal due to the harmonics caused by non-linear loads and speed variations. The proposed method allows rejecting the load-related components and other undesired frequencies to make the calculation of partial demagnetization signature for maximizing the performance of fault detection easier in a double structural AFPM generator independently of the load and speed variations. As it has been demonstrated, the faulty frequencies can be detected and tracked perfectly without using any extra electronics. Moreover, as shown in the diagrammatic presentation of results, the energy of the IMFs' increases with respect to

fault severity and the demagnetization degree can be evaluated based on the IMFs energy value. The proposed approach could be developed to detect several axial flux machine fault signatures such as static and dynamic eccentricity and inter-turn short circuit faults.

List of Symbols and Abbreviations

AFPM, axial flux permanent magnet; **IMF**, intrinsic mode functions; **EMD**, empirical mode decomposition; **IA**, instantaneous amplitude; **IF**, Instantaneous Frequency; **MCSA**, Machine Current Signature Analysis; **TMCSA**, Transient Machine Current Signature Analysis; **FFT**, Fast Fourier Transform; **STFT**, Short Time Fourier Transform; **HHT**, Hilbert-Huang Transform; **EMF**, Electromotive Force; $\mathbf{\Lambda_{dmg}}$, The permeance due to one partial demagnetized magnet; **MMF**, Magneto motive Force, $\mathbf{F_m}$, Magnetic-field Motion Force; $\boldsymbol{\mu_0}$, The free space permeability of the flux path; $\boldsymbol{\omega}$, The fundamental frequency in rad/sec; **P**, The number of pole pairs; $\mathbf{B_{AG(dmg)}}$, The air-gap magnetic flux density due to one partial demagnetized magnet; $\mathbf{V_{dmg}}$, The induced voltage in the stator coils due to the demagnetization; **rpm**, Round per minute; $\mathbf{f_s}$, Fundamental frequency; $\mathbf{e_{min}[n]}$, local minima points in sampled data; $\mathbf{e_{max}[n]}$, local maxima points in sampled data; $*$, points the convolution product; $\mathbf{T-F}$, time-frequency.

Reference

[1] F. TOOTOONCHIAN, K. ABBASZADEH and M. ARDEBILI, "Novel Axial Flux Brushless Resolver Analysis and Optimization using 3D Finite Element and D-Q Model Method," *Iranian Journal of Electrical & Electronic Engineering*, Vol. 8, No. 3, pp. 243–258, 2012.

[2] GHOLAMIAN S.A., ARDEBILI M. and ABBASZADEH K., "Analytic and FEM Evaluation of Power Density for Various Types of Double-Sided Axial Flux Slotted PM Motors," *International Journal of Applied Engineering Research*, Vol. 3, No. 6, pp. 749–762, 2008.

[3] XIA B., SHEN J.X., LUK P.C.K. and FEI W., "Comparative study of air cored axial-flux PM machines with different stator winding configurations," *IEEE Trans.Ind.Electron*, Vol. 62, No. 2, pp. 846-856, 2015.

[4] F. MAHMOUDITABAR, A. VAHEDI and P. OJAGHLU, "Investigation of Demagnetization Effect in an Interior V-Shaped Magnet Synchronous Motor at Dynamic and Static Conditions," *Iranian Journal of Electrical & Electronic Engineering*, Vol. 14, No. 1, pp. 22–27, 2018.

[5] LE ROUX, W. HARLEY R.G. AND HABETLER T.G., "Detecting Rotor Faults in Low Power Permanent Magnet Synchronous Machines," *IEEE Transactions on Power Electronics*, Vol. 38, No. 6, pp. 322-328, 2007.

[6] MA C., GAO Y., SUBRAMANI S., DEGANO M, WANG Y., FANG J., GERADA S.Z. and MU Y., "Eccentric position diagnosis of static eccentricity fault of external rotor permanent magnet synchronous motor as an in-wheel motor," *IET Electric Power Applications*, Vol. 14, No. 11, pp. 2263–2272, 2020.

[7] S.M. MIRIMANI, A. VAHEDI, F. MARIGNETTI and R.D. STEFANO, "An Online Method for Static Eccentricity Fault Detection in Axial Flux Machines," *IEEE Transactions on Industrial Electronics*, Vol. 62, No. 3, pp. 1931-1942, 2015.

[8] D.A. Y., SHI. X. and KRISHNAMURTHY M., "A New Approach to Fault Diagnostics for Permanent Magnet Synchronous Machines Using Electromagnetic Signature Analysis," *IEEE Transactions on Power Electronics*, Vol. 28, No. 8, pp. 4104-4112, 2013.

[9] PARK Y.et al., "Online Detection of Rotor Eccentricity and Demagnetization Faults in PMSMs Based on Hall-Effect Field Sensor Measurements," *IEEE Transactions on Industry Applications*, Vol. 55, No. 3, pp. 2499-2509, 2019.

[10] DONG L., JATSKEVICH J., HUANG Y., CHAPARIHA M. and LIU J., "Fault Diagnosis and Signal Reconstruction of Hall Sensors in Brushless Permanent Magnet Motor Drives," *IEEE Transactions on Energy Conversion*, Vol. 31, No. 1, pp. 118-131, 2016.

[11] ZHANG Q. and FENG M., "Fast Fault Diagnosis Method for Hall Sensors in Brushless DC Motor Drives," *IEEE Transactions on Power Electronics*, Vol. 34, No. 3, pp. 2585-2596, 2019.

[12] XIA. PENGPENG, YU. SHENBO, DOU. RUTONG and ZHAI FENGCHEN, "Analytical modeling and study on noise characteristics of rotor eccentric SPMSM with unequal magnetic poles structure," *Turkish Journal of Electrical Engineering and Computer Sciences*, Vol. 29, No. 2, Article 40, 2021.

[13] TORREGROSSA D., KHOOBROO A. and FAHIMI B., "Prediction of Acoustic Noise and Torque Pulsation in PM Synchronous Machines with Static Eccentricity and Partial Demagnetization Using Field Reconstruction Method," *IEEE Transactions on Industrial Electronics*, Vol. 59, No. 2, pp. 934-944, 2012.

[14] CHREIER L., BENDL J. and CHOMAT M., "Analysis of stator and rotor currents and torque of induction machine with rotor-bar faults," *Electr Eng*, Vol. 103, pp. 519–528, 2021.

[15] EBRAHIMI B.M. and FAIZ J., "Demagnetization Fault Diagnosis in Surface Mounted Permanent Magnet Synchronous Motors," *IEEE Transactions on Magnetics*, Vol. 49, No. 3, pp. 1185-1192, 2013.

[16] KE L.V., GAO C., SI J., FENG H. and CAO W., "Fault coil location of inter-turn short-circuit for direct-drive permanent magnet synchronous motor using knowledge

graph," *IET Electric Power Applications*, Vol. 14, No. 9, pp. 1712–1721, 2020.

[17] JONGMAN HONG., SANGUK PARK., DOOSOO HYUN., TAE-JUNE KANG., SANG BIN LEE., CHRISTIAN KRAL and ANTON HAUMER., "Detection and Classification of Rotor Demagnetization and Eccentricity Faults for PM Synchronous Motors," *IEEE Transactions on Industry Applications*, Vol. 48, No. 3, pp. 923-932, 2012.

[18] AKAR MEHMET., HEKİM MAHMUT. and ORHAN UMUT., "Mechanical fault detection in permanent magnet synchronous motors using equal width discretization-based probability distribution and a neural network model," *Turkish Journal of Electrical Engineering and Computer Sciences*, Vol. 23, No. 3, Article 14, 2015.

[19] EKER MUSTAFA and AKAR MEHMET., "Eccentricity fault diagnosis in a permanent magnet synchronous motor under nonstationary speed conditions," *Turkish Journal of Electrical Engineering and Computer Sciences*, Vol. 25, No. 3, Article 22, 2017.

[20] MAOUCHE Y., OUMAAMAR M.E.K. and BOUCHERMA M., "The Propagation Mechanism of Fault Signatures in Squirrel Cage Induction Motor Drives," *J. Electr. Eng. Technol*, Vol. 14, pp. 121–133, 2019.

[21] PONS-LLINARES J., ANTONINO-DAVIU J.A., RIERA-GUASP M., PINEDA-SANCHEZ M. and CLIMENTE-ALARCON V., "Induction Motor Diagnosis Based on a Transient Current Analytic Wavelet Transform via Frequency B-Splines," *IEEE Transactions on Industrial Electronics*, Vol. 58, No. 5, pp. 1530-1544, 2011.

[22] F. BAGHERI, H. KHALOOZADEH and K. ABBASZADEH, "Stator Fault Detection in Induction Machines by Parameter Estimation Using Adaptive Kalman Filter," *Iranian Journal of Electrical & Electronic Engineering*, Vol. 3, No. 3, pp. 72–82, 2007.

[23] ZANARDELLI W.G., STRANGAS E.G. and AVIYENTE S., "Identification of Intermittent Electrical and Mechanical Faults in Permanent-Magnet AC Drives Based on Time–Frequency Analysis," *IEEE Transactions on Industry Applications*, Vol. 43, No. 4, pp. 971-980, 2007.

[24] AKAR MEHMET., TAŞKIN SEZAİ, ŞEKER ŞAHİN SERHAT and ÇANKAYA İLYAS, "Detection of static eccentricity for permanent magnet synchronous motors using the coherence analysis," *Turkish Journal of Electrical Engineering and Computer Sciences*, Vol. 18, No. 6, Article 3, 2010.

[25] STRANGAS E.G., AVIYENTE S. and ZAIDI S.S.H., "Time–Frequency Analysis for Efficient Fault Diagnosis and Failure Prognosis for Interior Permanent-Magnet AC Motors," *IEEE Transactions on Industrial Electronics*, Vol. 55, No. 12, pp. 4191-4199, 2008.

[26] ABUBAKAR U., MEKHILEF S., GAEID K.S., MOKHLIS H. and ALMASHHADANY Y.I., "Induction motor fault detection based on multi-sensory control and wavelet analysis," *IET Electric Power Applications*, Vol. 14, No. 11, pp. 2051-2061, 2020.

[27] FAIZ J. and MAZAHERI-TEHRANI E., "Demagnetization Modelling and Fault Diagnosing Techniques in Permanent Magnet Machines under Stationary and Non-stationary Conditions, An Overview," *IEEE Transactions on Industry Applications*, Vol. 53, No. 3, pp. 2772-2785, 2017.

[28] VINAYAK B.A K. and JAGADANAND G., "Wavelet-based real-time stator fault detection of inverter-fed induction motor," *IET Electric Power Applications*, Vol. 14, No. 1, pp. 82-90, 2020.

[29] KAYA YILMAZ., KUNCAN FATMA. and ERTUNÇ HÜSEYİN METİN., "A new automatic bearing fault size diagnosis using time-frequency images of CWT and deep transfer learning methods," *Turkish Journal of Electrical Engineering and Computer Sciences*, Vol. 30, No. 5, Article 12, 2022.

[30] RAMU S.K., IRUDAYARAJ G.C.R., SUBRAMANI S. and SUBRAMANIAM U., "Broken rotor bar fault detection using Hilbert transform and neural networks applied to direct torque control of induction motor drive," *IET Power Electronics*, Vol. 13, No. 15, pp. 3328–3338, 2020.

[31] ELBOUCHIKHI, E., CHOQUEUSE V., AMIRAT Y., BENBOUZID M.E.H. and TURRI S., "An Efficient Hilbert Huang Transform-Based Bearing Faults Detection in Induction Machines," *IEEE Transactions on Energy Conversion*, Vol. 32, No. 2, pp. 401-413, 2017.

[32] WANG C., LIU X. and CHEN Z., "Incipient Stator Insulation Fault Detection of Permanent Magnet Synchronous Wind Generators Based on Hilbert–Huang Transformation," *IEEE Transactions on Magnetics*, Vol. 50, No. 1, pp. 1-4, 2014.

[33] ALVAREZ-GONZALEZ F., GRIFFO A. and WANG B., "Permanent magnet synchronous machine stator windings fault detection by Hilbert–Huang transform," T*he Journal of Engineering*, Vol. 2019, No. 17, pp. 3505-3509, 2019.

[34] TARAN N. and ARDEBILI M., "Multi-objective Optimal Design of an Axial Flux Permanent Magnet Generator for Directly Coupled Wind Turbines," *International Journal of Scientific and Engineering Research*, Vol. 5, No. 7, pp. 298-305, 2014.

[35] HUANG YUNKAI., GUO BAOCHENG., GUO YOUGUANG., ZHU JIANGUO., HEMEIDA AHMED. and SERGEANT PETER. "Analytical modeling of axial flux PM machines with eccentricities," *International*

Journal of Applied Electromagnetics and Mechanics, Vol. 53, No 4, pp. 1-21, 2016.

[36] RAJAGOPALAN S., ROUX W.L., T.G. HABETLER and HARLEY R.G., "Dynamic Eccentricity and Demagnetized Rotor Magnet Detection in Trapezoidal Flux (Brushless DC) Motors Operating Under Different Load Conditions," *IEEE Transactions on Power Electronics*, Vol. 22, No. 5, pp. 2061-2069, 2007.

[37] EBRAHIMI B.M., FAIZ J. and ROSHTKHARI M.J., "Static, Dynamic and Mixed Eccentricity Fault Diagnoses in Permanent-Magnet Synchronous Motors," *IEEE Transactions on Industrial Electronics*, Vol. 56, No. 11, pp. 4727-4739, 2009.

[38] DUAN Y. and TOLIYAT H., "A review of condition monitoring and fault diagnosis for permanent magnet machines," *IEEE Power and Energy Society General Meeting, San Diego, CA*, pp.1-4, 2012. Doi: 10.1109/PESGM.2012.6345545.

[39] Huang E., "Introduction to the Hilbert- Huang transform and its related mathematical problems," *Goddard Institute for Data Analysis*, Code, 614.2, NASA/Goddard Space Flight Center, Greenbelt, MD 20771, USA, 2014.

[40] NORDEN E.H., MAN-LI C.W., STEVEN R.L., SAMUEL S.P.S., WENDONG Q., PER GLOERSEN and KUANG L.F., "A confidence limit for the empirical mode decomposition and Hilbert spectral analysis," *Proceedings of the Royal Society A, Mathematical, Physical and Engineering Sciences*, Vol .459, No. 2037, pp. 2317-2345, 2003.

[41] VINAYAK B.A.K. and JAGADANAND G., "Wavelet-based real-time stator fault detection of inverter-fed induction motor," *IET Electric Power Applications*, Vol. 14, No. 1, pp.82 - 90, 2020.

[42] REHMAN A., Chen Y., Zhang M. and et al., "Fault detection and fault severity calculation for rotor windings based on spectral, wavelet and ratio computation analyses of rotor current signals for a doubly fed induction generator in wind turbines," *Electr Eng*, Vol.102, PP.1091–1102, February 2020.

[43] RAMU S.K., IRUDAYARAJ G.C.R., SUBRAMANI S. and SUBRAMANIAM U., "Broken rotor bar fault detection using Hilbert transform and neural networks applied to direct torque control of induction motor drive," *IET Power Electronics*, Vol. 13, No. 15. p.3328 – 3338, 2020.

[44] ELBOUCHIKHI E., CHOQUEUSE V., AMIRAT Y., BENBOUZID M.E.H. and TURRI S., "An Efficient Hilbert Huang Transform-Based Bearing Faults Detection in Induction Machines," *IEEE Transactions on Energy Conversion*, Vol.32, No.2. pp.401-413, June 2017.

[45] Wang C., Liu X. and Chen Z., "Incipient Stator Insulation Fault Detection of Permanent Magnet Synchronous Wind Generators Based on Hilbert–Huang Transformation," *IEEE Transactions on Magnetics*, Vol.50, No.11, pp.1-4, Nov.2014, Art No.8206504.

[46] Alvarez-Gonzalez F., GRIFFO A. and Wang B., "Permanent magnet synchronous machine stator windings fault detection by Hilbert–Huang transform," The *Journal of Engineering*, Vol.2019, No.17, pp.3505-3509, 2019.

[47] TARAN N. and ARDEBILI M., "Multi-objective Optimal Design of an Axial Flux Permanent Magnet Generator for Directly Coupled Wind Turbines," *International Journal of Scientific and Engineering Research*, Vol. 5, No. 7, 2014.

[48] K. N. GYFTAKIS., S. A. RASID., G. A. SKARMOUTSOS. and M. Mueller., "The Demagnetization Harmonics Generation Mechanism in Permanent Magnet Machines With Concentrated Windings," in *IEEE Transactions on Energy Conversion*, Vol. 36, No. 4, pp. 2934-2944, 2021.

[49] Huang E., "Introduction to the Hilbert- Huang transform and its related mathematical problems," *Goddard Institute for Data Analysis*, Code 614.2, NASA Space Flight Center, Greenbelt, MD 20771, USA.

[50] Huang NORDEN E., Wu Man-Li C., Long Steven R., Shen Samuel S.P., Qu WENDONG., GLOERSEN Per. and Fan KUANG L. "confidence limit for the empirical mode decomposition and Hilbert spectral analysis," *Proceedings of the Royal Society A: Mathematical, Physical and Engineering Sciences*, Vol.459, No. 2037, pp.2317-2345, 2003.

Yousef Alinejad-Beromi was born in Damghan, Iran. He received a B.Sc. degree in electrical engineering from K.N.T. University, Tehran, Iran, and an M.Sc. and Ph.D. degree from UWCC, (Wolfson Centre for Magnetic Technology), Cardiff, U.K., in 1989 and 1992, respectively. He is currently an Associate Professor with the Faculty of Electrical and Computer Science Engineering, at Semnan University, Semnan, Iran. His research interests include magnetic materials, electric generators, pulsed power supplies, and motor drives.

Makan Torabi was born in 1985 in Damghan, Iran. He received a B.Sc. degree and an M.Sc. degree from the Shahrood University of Technology, Shahrood, Iran, in 2013 and 2010, respectively and he is currently a Ph.D. student at Semnan University, Semnan, Iran. He is also with Semnan Province Electric Power Distribution Co, Semnan, Iran. His research interests include electric machinery, power electronics, and power system protection.